VOLUME 116, NUMBER 3
FEBRUARY 9, 1994

JOURNAL
OF THE
AMERICAN
CHEMICAL
SOCIETY

$[Fe(OMe)_2(O_2CCH_2Cl)]_{10}$, a Molecular Ferric Wheel

Kingsley L. Taft,[1a] Christopher D. Delfs,[1b] Georgia C. Papaefthymiou,[1c] Simon Foner,[1d] Dante Gatteschi,*[,1b] and Stephen J. Lippard*[,1a]

Contribution from the Department of Chemistry and the Francis Bitter National Magnet Laboratory, Massachusetts Institute of Technology, Cambridge, Massachusetts 02139, and the Dipartimento di Chimica, Universita' degli Studi di Firenze, Italia 50144

Received September 9, 1993®

Abstract: The synthesis of $[Fe(OMe)_2(O_2CCH_2Cl)]_{10}$, a molecular ferric wheel, from basic iron chloroacetate and ferric nitrate in methanol is described. Spectroscopic analysis of methanol solutions used to prepare the compound revealed a (μ-oxo)(μ-carboxylato)diiron(III) intermediate having terminal oxygen donor ligands. The structure of the crystalline ferric wheel was revealed in a single crystal X-ray diffraction investigation. The molecule has idealized D_{5d} symmetry and consists of a 20-membered ring comprised of 10 ferric ions linked by 20 bridging methoxide and 10 bridging chloroacetate ligands. The 10 iron atoms are approximately coplanar and are coordinated in a distorted octahedral manner by 6 oxygen donor atoms. Quantitative analysis of the geometry indicated that the curvature arises from a combination of convex bending by 205° (interior angle) across the bridging methoxides and concave bending by 119° (interior angle) at the iron atoms. The Mössbauer spectrum of a polycrystalline sample of the ferric wheel at 4.2 K consisted of a single quadrupole split doublet with $\delta = 0.52$ mm s^{-1} and $\Delta E_Q = 0.62$ mm s^{-1}. The solid state magnetic properties of the compound were extensively investigated. The χT value decreased from 32.3 emu mol^{-1} K at 300 K to 0.355 emu mol^{-1} K at 2.5 K, consistent with antiferromagnetic exchange coupling. The temperature dependence of the susceptibility could be adequately fit by a classical linear chain treatment down to 50 K with a nearest-neighbor coupling constant of $\sim$10 cm^{-1}, where $H = JS_iS_{i+1}$, and $g = 2.0$. In order to account for the temperature dependence over the entire temperature range, the Heisenberg–Dirac–van Vleck spin Hamiltonian was applied and solved numerically for a ring of eight iron(III) ions, an approach that gave $J = 9.6$ cm^{-1}, with $g = 2.0$, and an excellent fit to the experimental data. The low-lying states of the spin manifold were dramatically revealed by high-field DC and pulsed magnetization measurements at 0.6 K. The reduced magnetization increased in discrete steps with evenly spaced increments in the magnetic field, a result that was quantitatively accounted for by the theoretical spin manifold.

Introduction

The recent synthesis of polynuclear metal complexes with oxygen atom bridges has afforded a fascinating array of new molecules displaying a variety of unusual geometric symmetries and patterns.[2] Both the synthetic techniques used to access these compounds and the magnetic properties associated with a large number of interacting paramagnetic centers in a single cluster add to their interest.[3]

Iron(III) compounds occupy a central position in this field. Numerous naturally-occurring iron oxide minerals with extended

* Abstract published in *Advance ACS Abstracts*, January 15, 1994.

(1) (a) Massachusetts Institute of Technology Chemistry Department. (b) Universita' degli Studi di Firenze Dipartimento di Chimica. (c) Francis Bitter National Magnet Laboratory. (d) Francis Bitter National Magnet Laboratory and Massachusetts Institute of Technology Physics Department.

(2) (a) Lippard, S. J. *Angew. Chem., Int. Ed. Engl.* **1988**, *27*, 344. (b) Wieghardt, K. *Angew. Chem., Int. Ed. Engl.* **1989**, *28*, 1153. (c) Hagen, K. S. *Angew. Chem., Int. Ed. Engl.* **1992**, *31*, 1010.

(3) Gatteschi, D.; Pardi, L.; Sessoli, R. *Mater. Sci.* **1991**, *17*, 7.

0002-7863/94/1516-0823$04.50/0

structures are known,[4,5] and a biological manifestation of these inorganic systems, the iron storage protein ferritin, has been studied extensively.[6] Discrete molecules with up to 19 iron atoms and bridging oxygen ligands have been synthesized and characterized.[7-12]

In the present article we describe the synthesis, geometry, and Mössbauer and magnetic properties of a unique member of this class, $[Fe(OMe)_2(O_2CCH_2Cl)]_{10}$ (**1**), a circular decanuclear iron(III) complex with bridging methoxide and carboxylate ligands. Inspired by its remarkable structure, we refer to this compound as a molecular "ferric wheel".[13] The high symmetry of **1** facilitates the analysis of its magnetic behavior in a manner not previously possible for such a large collection of unpaired spins. Moreover, this compound should be of interest to people working in the area of one-dimensional magnetism since it affords an opportunity to compare the experimentally observed properties of a large ring with those of chains. Previously, theories developed for analyzing magnetically coupled ring systems have been extensively applied to calculate the thermodynamic properties of one-dimensional materials.[14,15]

Experimental Section

The basic iron monochloroacetate, $[Fe_3O(O_2CCH_2Cl)_6(H_2O)_3](NO_3)\cdot 4H_2O$, was prepared as described previously.[16] All other reagents were obtained from commercial sources and used without further purification.

Synthesis of $[Fe(OMe)_2(O_2CCH_2Cl)]_{10}$ (1). To 0.342 g (0.367 mmol) of $[Fe_3O(O_2CCH_2Cl)_6(H_2O)_3](NO_3)\cdot 4H_2O$ and 0.444 g (1.10 mmol, 3 equiv) of $Fe(NO_3)_3\cdot 9H_2O$ was added 50 mL of methanol. After being stirred for a few minutes, the green-brown solution was filtered to remove a small amount of undissolved iron salts. Vapor diffusion of anhydrous diethyl ether into the solution turned it yellow in color and, after 1 week, gold crystals of **1** formed along with a yellow powder and a colorless microcrystalline solid. In the most efficient method of preparing **1**, which gave the largest crystals and best yields, the original reaction solution was divided into 10 equal 5-mL portions. During the crystallization period, the total volume of each aliquot increased to approximately 20 mL, and these separate batches were then combined prior to the isolation of **1**. The two impurities were removed by decanting away a slurry of the yellow powder and dissolving the clear compound in large amounts of methanol. Typical preparations gave 0.080 g of $[Fe(OMe)_2(O_2CCH_2Cl)]_{10}$ (**1**), 17% based on iron. Anal. Calcd for $C_{40}H_{80}O_{40}Fe_{10}Cl_{10}$ (**1**): C, 22.73; H, 3.81; Fe, 26.42. Found: C, 22.67; H, 3.82; Fe, 26.14. IR (KBr, cm^{-1}): 2926, 2824, 1561 (ν_{as}, COO), 1419 (ν_s, COO), 1255, 1034 (ν, OMe), 794, 708, 508, 444. Compound **1** hydrolyzes in moist air to give a red solid, the elemental composition and IR spectroscopic properties of which are consistent with the empirical formulation $[Fe(OH)_2(O_2CCH_2Cl)]$. Anal. Calcd for $C_2H_4O_4FeCl$: C, 13.10; H, 2.20. Found: C, 12.75; H, 2.30. IR (KBr, cm^{-1}): 3430 (ν, OH), 1560 (ν_{as}, COO), 1418 (ν_s, COO), 1256, 940, 796, 695.

Table 1. Crystallographic Information for $[Fe(OMe)_2(O_2CCH_2Cl)]_{10}$ (**1**)[a]

formula	$Fe_{10}C_{40}H_{80}O_{40}Cl_{10}$
fw	2114.06
cryst syst	monoclinic
space group[b]	$P2_1/c$ (No. 14)
a, Å	11.106(3)
b, Å	15.958(3)
c, Å	22.938(5)
β, deg	97.34(1)
V, Å^3	4032(1)
Z	2
d_{calcd}, g/cm^3	1.74
T, K	226
data collctn range, deg	$3 \le 2\theta \le 50$
data limits	$\pm h,+k,+l$
no. of data collected	8174
R_{av}	0.032
no. of unique data	7352
no. obs unique data[c]	5043
no. of parameters	451
data/parameter ratio	11.2
abs coeff, cm^{-1}	21.60
transmission coeff, min/max	0.83/1.00
R^d	0.049
$R_w{}^d$	0.060
largest shift/esd, final	0.001
largest peak, e$^-$/Å^3	0.90

[a] All measurements were made by using an Enraf Nonius CAD-4F κ-geometry diffractometer and Mo Kα (0.71069 Å) radiation. [b] Hahn, T., Ed. *International Tables for X-ray Crystallography*; D. Reidel: Dordrecht, The Netherlands, 1983. [c] Observation criterion: $I > 3\sigma(I)$. [d] $R = \sum||F_o| - |F_c||/\sum|F_o|$, and $R_w = [\sum w(|F_o| - |F_c|)^2/\sum w|F_o|^2]^{1/2}$, where $w = 1/\sigma^2(F)$ and $\sigma^2(F)$ is defined in ref 17.

X-ray Crystallography. A golden crystal of **1** with dimensions 0.16 × 0.23 × 0.30 mm was mounted on the end of a quartz fiber with epoxy resin. X-ray data were collected and reduced by procedures previously documented,[17] details of which are given in Table 1. The quality of the crystal was excellent, with $\Delta\bar{\omega}_{1/2} = 0.20°$ for several intense, low-angle reflections. No crystal decay occurred during the data collection. The Laue symmetry and systematic absences were consistent with space group $P2_1/c$. Initial atomic coordinates for the five iron atoms in the asymmetric unit of **1** were determined by SHELXS-86.[18] Other non-hydrogen atoms were located from DIRDIF phase refinements and difference Fourier maps,[19] and the structure was refined by using the TEXSAN crystallographic software package.[20] An empirical absorption correction based on φ-scans was applied.[21] The iron, carbon, oxygen, and chlorine atoms were refined anisotropically, whereas the hydrogen atoms were generated with thermal parameters equal to 1.2 × B_{eq} of the parent carbon atom and carbon–hydrogen distances constrained to 0.95 Å. In the final stages of refinement, the methyl groups of the bridging methoxides directed into the ring center, C(1), C(3), C(5), C(7), and C(9), were observed to have oblong thermal ellipsoids with large values of B_{eq}. Examination of

(4) (a) Murad, E.; Johnston, J. H. In *Mössbauer Spectroscopy Applied to Inorganic Chemistry*; Long, G. J., Ed.; Plenum: New York, 1987; Vol. 2, pp 507–582. (b) Murray, J. W. In *Marine Minerals*; Burns, R. G., Ed.; Mineralogical Society of America: Washington, DC, 1979; pp 47–98.

(5) Flynn, C. M., Jr. *Chem. Rev.* **1984**, *84*, 31.

(6) (a) *Biomineralization: Chemical and Biochemical Perspectives*; Mann, S., Webb, J., Williams, R. J. P., Eds.; VCH: New York, 1989; pp 257–344. (b) Artymiuk, P. J.; Bauminger, E. R.; Harrison, P. M.; Lawson, D. M.; Nowik, I.; Treffry, A.; Yewdall, S. J. In *Iron Biominerals*; Frankel, R. B., Blakemore, R. P., Ed.; Plenum: New York, 1991; pp 269–294. (c) Crichton, R. R. *Inorganic Biochemistry of Iron Metabolism*; Horwood: New York, 1991.

(7) Discrete, structurally characterized complexes having six iron atoms are Fe_6: (a) Gérbéléu, N. V.; Batsanov, A. S.; Timko, G. A.; Struchkov, Y. T.; Indrichan, K. M.; Popovich, G. A. *Dokl. Akad. Nauk SSSR* **1987**, *293*, 122. (b) Micklitz, W.; Lippard, S. J. *Inorg. Chem.* **1988**, *27*, 3067. (c) Micklitz, W.; Bott, S. G.; Bentsen, J. G.; Lippard, S. J. *J. Am. Chem. Soc.* **1989**, *111*, 372. (d) Hegetschweiler, K.; Schmalle, H.; Streit, H. M.; Schneider, W. *Inorg. Chem.* **1990**, *29*, 3625. (e) McCusker, J. K.; Christmas, C. A.; Hagen, P. M.; Chadha, R. K.; Harvey, D. F.; Hendrickson, D. N. *J. Am. Chem. Soc.* **1991**, *113*, 6114. (f) Hegetschweiler, K.; Schmalle, H. W.; Streit, H. M.; Gramlich, V.; Hund, H.-U.; Erni, I. *Inorg. Chem.* **1992**, *31*, 1299. (g) Hagen, K. S.; Nair, V. S. *Inorg. Chem.* **1992**, *31*, 4048. (h) Harding, C. J.; Henderson, R. K.; Powell, A. K. *Angew. Chem., Int. Ed. Engl.* **1993**, *32*, 570.

(8) Fe_8: Wieghardt, K.; Pohl, K.; Jibril, I.; Huttner, G. *Angew. Chem., Int. Ed. Engl.* **1984**, *23*, 77. (b) Delfs, C. D.; Gatteschi, D.; Pardi, L.; Sessoli, R.; Wieghardt, K.; Hanke, D. *Inorg. Chem.* **1993**, *32*, 3099.

(9) Fe_{11}: Gorun, S. M.; Papaefthymiou, G. C.; Frankel, R. B.; Lippard, S. J. *J. Am. Chem. Soc.* **1987**, *109*, 3337.

(10) Fe_{12}: Taft, K. L.; Papaefthymiou, G. C.; Lippard, S. J. *Science* **1993**, *259*, 1302.

(11) $Fe_{16}M$, M = Mn(II), Co(II), or Fe(II): (a) Micklitz, W.; Lippard, S. J. *J. Am. Chem. Soc.* **1989**, *111*, 6856. (b) Micklitz, W.; McKee, V.; Rardin, R. L.; Pence, L. E.; Lippard, S. J. Submitted for publication.

(12) Fe_{17}, Fe_{19}: Heath, S. L.; Powell, A. K. *Angew. Chem., Int. Ed. Engl.* **1992**, *31*, 191.

(13) Taft, K. L.; Lippard, S. J. *J. Am. Chem. Soc.* **1990**, *112*, 9629.

(14) (a) O'Connor, C. J. *Prog. Inorg. Chem.* **1982**, *29*, 203. (b) Carlin, R. L. *Magnetochemistry*; Springer-Verlag: New York, 1986.

(15) De Jongh, L. J.; Miedema, A. R. *Adv. Phys.* **1974**, *23*, 1.

(16) Taft, K. L.; Garfinkel-Shweky, D.; Masschelein, A.; Liu, S.; Bino, A.; Lippard, S. J. *Inorg. Chim. Acta* **1992**, *198–200*, 627.

(17) Carnahan, E. M.; Rardin, R. L.; Bott, S. G.; Lippard, S. J. *Inorg. Chem.* **1992**, *31*, 5193.

(18) Sheldrick, G. M. In *Crystallographic Computing*; Sheldrick, G.M., Krüger, C., Goddard, R., Ed.; Oxford University Press: Oxford, 1985; p 175.

(19) Pathasarathi, V.; Beurskens, P. T.; Slot, J. J. B. *Acta Crystallogr.* **1983**, *A39*, 860.

(20) *TEXSAN: Single Crystal Structure Analysis Software, Version 5.0*; Molecular Structure Corporation: The Woodlands, TX, 1989.

(21) North, A. C. T.; Phillips, D. C.; Mathews, F. S. *Acta Crystallogr.* **1968**, *A24*, 351.

difference Fourier maps in the regions of these atoms revealed an electron density distribution which was not amenable to refinement based on a disordered model having discrete atomic positions. A small amount of residual electron density (0.8 $e^-/Å^3$) was located on the inversion center in the center of the ring at $^1/_2, 0, ^1/_2$. The largest unaccounted for peak in the final difference Fourier map, 0.90 $e^-/Å^3$, was adjacent to C(1). Final atomic positional and thermal parameters and all unique bond distances and angles are available as supplementary material.

Physical Measurements. Fourier transform infrared spectra of samples pressed into KBr were recorded on a Bio-Rad SPC3200 instrument. Raman spectra were acquired with a Kr^+ laser at 406.7 nm. A high-resolution double monochromator and an optical multichannel analyzer were employed in a standard back-scattering configuration. The methanol solution, loaded in a NMR tube, was spun during data collection. Twenty scans were averaged, and a baseline correction was applied. A holographic Raman edge filter was used to attenuate Rayleigh scattering. The wavelengths of the spectral window were referenced versus chloroform.

The Mössbauer spectrum of microcrystalline **1**, dispersed in BN, was measured at the Francis Bitter National Magnet Laboratory at 4.2 K. A conventional constant acceleration spectrometer was equipped with a temperature controller maintaining temperatures within 0.1 K and a γ-ray source of ^{57}Co in Rh maintained at room temperature. Isomer shifts were referenced versus iron metal at 300 K.

Variable-temperature magnetic measurements of microcrystalline **1** were made by using a Quantum Design SQUID susceptometer in the Department of Material Science and Engineering at M.I.T. Fifty-six data points between 2.5 and 300 K were collected at 3 and 9 kG on a 0.0773-g sample. The experimental emu was corrected for both the magnetism of the sample holder, a bucket constructed from the polymer Kel-F, and a diamagnetic contribution of -9.4×10^{-4} emu mol^{-1} for the molecule, as calculated from Pascal's constants.[14] Measurements at the two fields gave nearly identical χ values in the temperature range investigated.

DC magnetization studies of **1** at 4.2 and 0.6 K from 0 to 20 tesla were performed at the Francis Bitter National Magnet Laboratory. A vibrating sample magnetometer (VSM) equipped with a $^4He/^3He$ cooling system and surrounded by a water-cooled Bitter electromagnet was employed.[22] The VSM, a Princeton Applied Research instrument, was modified for operation in the high-field, water-cooled facilities. A sample of **1** weighing 0.0151 g was compressed in a Teflon bucket containing N_2 gas with a plunger rod assembly. The large magnetic fields achieved in the experiment produced correspondingly large emu values, and no corrections were made for the sample holder nor underlying diamagnetism. Carbon and hydrogen analyses of the two samples of **1** used in the variable-temperature and high-field magnetic measurements were within 0.2% of the calculated values.

Pulsed-field magnetic experiments up to 50 tesla at 0.6 K were conducted at the Francis Bitter National Magnet Laboratory. The magnets, cryogenic and detection systems, and data acquisition and processing procedures have been previously described.[23] The sample holder was similar to the one employed in the DC magnetization studies. The differential magnetization of a 0.0070-g sample of **1** as a function of field was measured for a range of field sweeps.

Results and Discussion

Synthesis. Polyiron oxo carboxylato complexes can be obtained by the controlled hydrolysis of basic iron carboxylates.[2a,c] The chemistry of this triangular (μ-oxo)hexakis(μ-carboxylato)triiron(III) unit has been reviewed.[24] Hydrolysis of the benzoate derivative in acetonitrile has provided the largest aggregates, including undecanuclear and heptadecanuclear clusters.[9,11] In these reactions, the $\{Fe_3O\}^{7+}$ core of the basic iron carboxylate serves as a building block for higher nuclearity species. Basic iron carboxylates have also been used as starting materials in the synthesis of low nuclearity model complexes for the active sites of the metalloproteins hemerythrin and ribonucleotide reductase,[16,25] both of which contain (μ-oxo)(μ-carboxylato)diiron(III) centers in their oxidized forms.[26] For example, addition of the bidentate nitrogen donor ligand BIPhMe to a methanol solution of basic iron acetate and ferric nitrate generated the desired diiron(III) core.[16,27] Here the $\{Fe_3O\}^{7+}$ unit formally lost a ferric ion in the isolated product. When the reaction was carried out in methanol without a bidentate chelating ligand, eq 1, the ferric wheel **1** was obtained. By eliminating BIPhMe, a nonbridging ligand that terminates the growth of a high nuclearity complex, **1** was able to assemble. Several high-nuclearity iron–sulfur and –selenium complexes have been obtained by following a similar strategy.[28]

$$[Fe_3O(O_2CCH_2Cl)_6(H_2O)_3](NO_3) + 3Fe(NO_3)_3 \xrightarrow{MeOH} \xrightarrow{Et_2O} \underset{\mathbf{1}}{[Fe(OMe)_2(O_2CCH_2Cl)]_{10}} \quad (1)$$

The green-brown color of the initial reaction solution resembled that of complexes containing the (μ-oxo)(μ-carboxylato)diiron(III) core.[29] The electronic spectrum of this methanol solution had a shoulder at 620 nm, a feature characteristic of the (μ-oxo)diiron(III) unit with at least one bridging carboxylate ligand (Figure S1, supplementary material). This absorption has been assigned as either a ligand field or a ligand → metal charge transfer transition.[30] Regardless of its origin, the energy of this band is useful for identifying the terminal ligands coordinated to the (μ-oxo)(μ-carboxylato)diiron(III) core.[29] A coordination environment comprised only of oxygen donors gives values near 600 nm,[31] whereas the absorption band falls between 700 and 750 nm when the ligands are all nitrogen donors.[32] The spectrum of the solution from which **1** ultimately precipitated was characteristic of a (μ-oxo)(μ-carboxylato)diiron(III) species having an all oxygen atom coordination environment. Potential terminal ligands include methanol, nitrate, or carboxylate, all three of which are known in crystallographically characterized complexes of this class.[16,33-35]

A band at 534 cm^{-1}, assigned to the ν_s(Fe–O–Fe) stretch, in the Raman spectrum of the methanol reaction solution confirmed the existence of a (μ-oxo)(μ-carboxylato)diiron(III) complex (Figure S2, supplementary material). The energy of this diagnostic signal depends on the Fe–O–Fe angle, a value of 534 cm^{-1} corresponding to an Fe–O–Fe angle of 120°.[36] This angle is consistent with at least one, and possibly two, carboxylate bridges in addition to the μ-oxo ligand.[29]

Attempts to isolate a green (μ-oxo)(μ-carboxylato)diiron(III) complex from the reaction solution were unsuccessful, however.

(22) Foner, S. *Rev. Sci. Instrum.* **1959**, *30*, 548.
(23) Foner, S.; Shapira, Y.; Heiman, D.; Becla, P.; Kershaw, R.; Dwight, K.; Wold, A. *Phys. Rev. B* **1989**, *39*, 11793.
(24) Cannon, R. D.; White, R. P. *Prog. Inorg. Chem.* **1988**, *36*, 195.
(25) (a) Nishida, Y.; Haga, S.; Tokil, T. *Chem. Lett.* **1989**, 109. (b) Nishida, Y.; Nasu, M.; Tokii, T. *Inorg. Chim. Acta* **1990**, *169*, 143.
(26) Que, L., Jr.; True, A. E. *Prog. Inorg. Chem.* **1990**, *38*, 97.
(27) Abbreviations: acacH, acetylacetone; biphenH_2, 1,1′-biphenyl-2,2′-diol; BIPhMe, 2,2′-bis(1-methylimidazol-2-yl)phenylmethoxymethane; catH_2, catechol; N(PL)$_2$alaH_2, α-3-dihydroxy-β-[[[3-hydroxy-5-(hydroxymethyl)-2-methyl-4-pyridyl]methylene]amino]-5-(hydroxymethyl)-α,2-dimethyl-4-pyridinepropanoic acid; Hdmpz, 3,5-dimethylpyrazole; LH_2, *N,N′*-ethylenebis(salicylamine); heidiH_3, *N*-(2-hydroxyethyl)iminodiacetic acid; salpaH_2, *N*-(3-hydroxypropyl)salicylaldimine; dipicH_2, 2,6-pyridinedicarboxylic acid; Me_3tacn, 1,4,7-trimethyl-1,4,7-triazacyclononane; tren, tris(2-aminoethyl)amine; XDKH_2, xylenediaminebis(Kemp's triacid imide).
(28) (a) You, J.-F.; Snyder, B. S.; Papaefthymiou, G. C.; Holm, R. H. *J. Am. Chem. Soc.* **1990**, *112*, 1067. (b) You, J.-F.; Papaefthymiou, G. C.; Holm, R. H. *J. Am. Chem. Soc.* **1992**, *114*, 2697.
(29) Kurtz, D. M., Jr. *Chem. Rev.* **1990**, *90*, 585.
(30) (a) Reem, R. C.; McCormick, J. M.; Richardson, D. E.; Devlin, F. J.; Stephens, P. J.; Musselman, R. L.; Solomon, E. I. *J. Am. Chem. Soc.* **1989**, *111*, 4688. (b) Ménage, S.; Que, L., Jr. *New J. Chem.* **1991**, *15*, 431.
(31) Feng, X.; Bott, S. G.; Lippard, S. J. *J. Am. Chem. Soc.* **1989**, *111*, 8046.
(32) Armstrong, W. H.; Spool, A.; Papaefthymiou, G. C.; Frankel, R. B.; Lippard, S. J. *J. Am. Chem. Soc.* **1984**, *106*, 3653.
(33) Tolman, W. B.; Liu, S.; Bentsen, J. G.; Lippard, S. J. *J. Am. Chem. Soc.* **1991**, *113*, 152.
(34) Sessler, J. L.; Hugdahl, J. D.; Lynch, V.; Davis, B. *Inorg. Chem.* **1991**, *30*, 336.
(35) Watton, S.P.; Masschelein, A.; Rebek, J., Jr.; Lippard, S. J. Unpublished results.
(36) Sanders-Loehr, J.; Wheeler, W. D.; Shiemke, A. K.; Averill, B. A.; Loehr, T. M. *J. Am. Chem. Soc.* **1989**, *111*, 8084.

Such a unit, having no chelating terminal ligands, has not yet been prepared with simple carboxylates. A (μ-hydroxy)bis(μ-formato)dichromium(III) complex with six terminal water ligands has been isolated and structurally characterized in the solid state, but even this relatively kinetically inert chromium(III) species readily converts in aqueous solution above 50 °C to the more stable basic chromium carboxylate.[37] A (μ-oxo)bis(μ-carboxylato)diiron(III) compound with all terminal solvent ligands has recently been synthesized from ferric nitrate and the dinucleating dicarboxylate ligand XDK^{2-} in methanol.[35] The rigid geometry of XDK^{2-} appears to stabilize the diiron core in a manner not yet achieved with unrestrained carboxylate ligands.

Vapor diffusion of large amounts of diethyl ether into the reaction solution resulted in a yellow color, and gold crystals of **1** formed over a period of 1 week. A yellow powder and a small amount of clear microcrystals also precipitated. The best yields of **1** were obtained when large amounts of diethyl ether were used, and attempts to improve the efficiency of the reaction by increasing the iron concentration produced more yellow powder and less **1**. Under the optimized reaction conditions, the iron concentration was ~0.015 M when crystals appeared. As in other cyclization reactions, closure of the 20-membered ring appears to require dilute solutions.

Neither **1** nor the yellow powder, which is presumably a polymeric iron(III) material, was soluble in any common organic solvents. During the washing stage, the purity of **1** was checked both visually and by IR spectroscopy. The yield of **1** is modest, only 17% with respect to iron, although a significant amount of crystalline product was lost in the purification steps. Attempts to increase the yield by adding various bases such as triethylamine to deprotonate methanol were unsuccessful. Complex **1** hydrolyzed in moist air over several hours to give an orange powder having the composition $[Fe(OH)_2(O_2CCH_2Cl)]$, as indicated by IR spectroscopy and elemental analysis. The substitution of alkoxide by hydroxide in the solid-state substitution has been observed,[7f,g] but the resulting solid was amorphous and its structure could not be determined.

The synthetic chemistry of iron(III)–alkoxides has been previously investigated.[38] Yellow solids with an empirical composition of $[Fe(OR)_2(O_2CR)]$ have been reported, and structures were suggested to explain their physical properties. No X-ray investigations were completed, however. The interaction of iron oxides with polyalcohols in aqueous solution has also been the subject of several studies, and a number of high-nuclearity polyiron species have been postulated to exist in solution.[39] In some respects, the chemistry of iron(III) in alcohol resembles its hydrolytic reactions.[5,40] Above pH 3, aqueous solutions of ferric ion readily form hydroxo and oxo-bridged dimers followed by precipitation of insoluble iron–oxide–hydroxides.[5,41] Such polymerization processes appear to be occurring in alcohol solutions of iron carboxylates as well. The extent of methanolysis, however, is mitigated by the alkyl substituent, which limits the bridging capacity of the oxygen atom. Methanol can only be deprotonated once and can, at most, bridge three metal ions. Bridging oxo ligands derived from water, by contrast, can link up to six metal ions. The high coordination numbers attained by μ-oxo anions and the ability of μ-hydroxo ligands to form hydrogen bonds give rise to a large variety of solid-state iron–oxide–hydroxides.[4,5] Alkoxide-bridged species are less extensively polymerized, and discrete molecules can be more readily crystallized and characterized. Polyiron alkoxide complexes containing four,[42] six,[7d,f,g] and twelve iron atoms[10] have recently been reported.

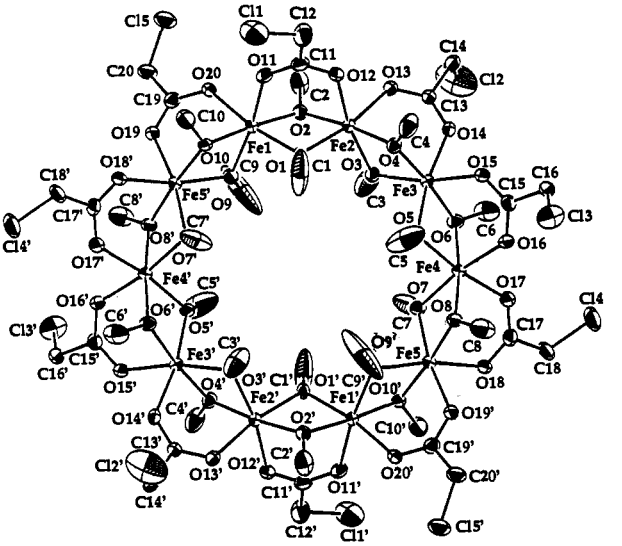

Figure 1. ORTEP view perpendicular to the plane of iron atoms in **1** showing the 50% probability thermal ellipsoids. Hydrogen atoms are omitted for clarity. Primed and unprimed atoms are related by a crystallographically-imposed center of symmetry.

Despite these insights, the exact mechanism of the ferric wheel formation remains uncertain. The color change to yellow accompanying the addition of diethyl ether signals the formation of (μ-OMe)iron(III) species, but identification of metal oligomers in the assembly of the ring has not been possible. The role of the (μ-oxo)(μ-carboxylato)diiron(III) complex observed in the initial reaction solution is also unknown. The lack of mechanistic information about the formation of **1**, however, is not unusual; the processes by which most high-nuclearity metal complexes form in solution remain obscure.

Structure. An ORTEP plot of the ferric wheel viewed perpendicular to the plane of the ring is depicted in Figure 1. The molecule contains ten octahedrally coordinated iron atoms linked in a large 20-membered ring by 20 methoxide and 10 carboxylate bridging ligands. There is a crystallographically imposed center of symmetry at the center of the wheel, although the molecule has virtual D_{5d} symmetry (see below). The bridging methoxide ligands can be subdivided into two sets, one pointing inward and one directed outward, like the bridging monochloroacetate ligands. This repetitive pattern in combination with a slight bend at the iron and bridging oxygen atoms produces the observed circular structure. The ten iron atoms lie within ±0.009 Å of a common plane. A view that emphasizes the toroidal shape of **1** is provided in Figure 2.

The iron atoms have almost identical coordination geometries. The average Fe–O bond lengths and O–Fe–O angles for the five unique sites are compiled in Table 2, with labels for the Fe(1) center used to identify specific geometric features. From the estimated standard deviations it is clear that the coordination geometry of all ten iron atoms is identical within the precision of the X-ray diffraction experiment. Variations among the Fe–O bond lengths, the Fe–OMe distances being approximately 0.1 Å shorter than the Fe–O_2CCH_2Cl distances, and the MeO–Fe–OMe angle of 78.0(2)° slightly distort the octahedral geometry. All three ligand types, the interior methoxides, the exterior methoxides, and the monochloroacetates, are disposed in an alternating fashion above and below the plane of the ring. The only atoms that do not strictly adhere to this pattern are the

(37) Turowski, P. N.; Bino, A.; Lippard, S. J. *Angew. Chem., Int. Ed. Engl.* **1990**, *29*, 811.
(38) (a) Kokot, E.; Mockler, G. M.; Sefton, G. L. *Aust. J. Chem.* **1973**, *26*, 2105. (b) Trzeciak, A.; Szymanska-Buzar, T.; Ziolkowski, J. J. *Polish J. Chem.* **1979**, *53*, 981.
(39) Rich, H. W.; Hegetschweiler, K.; Streit, H. M.; Erni, I.; Schneider, W. *Inorg. Chim. Acta* **1991**, *187*, 9, and references therein.
(40) (a) Schneider, W. *Comments Inorg. Chem.* **1984**, *3*, 205. (b) Schneider, W. *CHIMIA* **1988**, *42*, 9.
(41) Spiro, T. G.; Allerton, S. E.; Renner, J.; Terzis, A.; Bils, R.; Saltman, P. *J. Am. Chem. Soc.* **1966**, *88*, 2721.
(42) Taft, K. L.; Caneschi, A.; Pence, L. E.; Delfs, C. D.; Papaefthymiou, G. C.; Lippard, S. J. *J. Am. Chem. Soc.* **1993**, *115*, 11753.

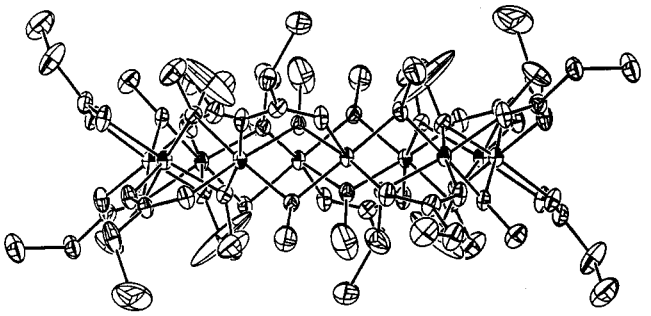

Figure 2. ORTEP view parallel to the plane of iron atoms of **1** showing 50% probability thermal ellipsoids. Hydrogen atoms are omitted for clarity.

Table 2. Average Interatomic Distances (Å) and Angles (deg) for $[Fe(OMe)_2(O_2CCH_2Cl)]_{10}$ (**1**)[a]

Fe(1)–O(1)	1.975(4)	O(1)–C(1)	1.39(2)	O(11)–C(11)	1.259(8)
Fe(1)–O(2)	1.987(6)	O(2)–C(2)	1.42(1)	C(11)–C(12)	1.51(1)
Fe(1)–O(11)	2.07(1)			C(12)–Cl(1)	1.76(3)

O(1)–Fe(1)–O(2)	78.0(2)	Fe(1)–O(1)–Fe(2)	100.0(4)
O(1)–Fe(1)–O(9)	98(1)	Fe(1)–O(1)–C(1)	125(2)
O(1)–Fe(1)–O(10)	98.4(9)	Fe(1)–O(2)–Fe(2)	99.3(4)
O(1)–Fe(1)–O(11)	88.5(8)	Fe(1)–O(2)–C(2)	126(1)
O(1)–Fe(1)–O(20)	169.3(8)	Fe(1)–O(11)–C(11)	127.1(8)
O(2)–Fe(1)–O(10)	174.4(9)	O(11)–C(11)–O(12)	127.0(5)
O(2)–Fe(1)–O(11)	91.1(6)	O(11)–C(11)–C(12)	116(3)
O(2)–Fe(1)–O(20)	92.9(9)	C(11)–C(12)–Cl(1)	112(2)
O(11)–Fe(1)–O(20)	86(2)		

Average Fe···Fe Distances

nearest neighbor	example	distance
first	Fe(1)–Fe(2)	3.028(4)
second	Fe(1)–Fe(3)	5.76(1)
third	Fe(1)–Fe(4)	7.93(2)
fourth	Fe(1)–Fe(5)	9.32(1)
fifth	Fe(1)–Fe(1)′	9.80(3)

[a] Numbers in parentheses are estimated standard deviations in the least significant digit. Primed and unprimed atoms are related by the crystallographically-imposed center of symmetry.

chlorine atoms of the carboxylate bridges, which adopt various orientations on the rim of the wheel. The staggered arrangement of alkoxide and carboxylate ligands produces a molecular C_5 axis, passing through the inversion center in the middle of the molecule, and there are five perpendicular C_2 axes through pairs of iron atoms related by the inversion center. The ferric wheel therefore has idealized D_{5d} molecular symmetry, the ten iron atoms being related by an S_{10} symmetry element. The high symmetry of **1** can be further appreciated by examining the Fe···Fe separations around the ring, the average values of which are included in Table 2. The distances are almost identical for each nearest-neighbor, second nearest-neighbor, etc. type.

A variety of diiron(III) complexes exist with two alkoxide,[43] hydroxide,[44] or aryloxide bridges,[45] or combinations thereof.[46] Several representative examples are listed in Table 3 together with their relevant geometric parameters. In contrast, complexes of this kind having an additional carboxylate bridge are rare, with only a single example, $(Hpip)_3[Fe_2(cat)_4(OAc)]$, having been structurally characterized.[47] The Fe–OR distances for the alkoxide- and hydroxide-bridged structures are quite similar, whereas the aryloxide and catecholate bridge distances are slightly longer, probably as a consequence of their lower basicity. The Fe···Fe distances for the dialkoxide bridged cores range from 3.089(6) Å for $[Fe(salpa)Cl]_2$ to over 3.217(7) Å for $[Fe_2(salpa)_2(salpah)_2]$. The metal–metal separations for **1** average 3.028(4) Å, a significantly shorter value resulting from the presence of the third, monochloroacetate bridge.

The majority of bis(μ-OR)diiron(III) complexes have crystallographically-imposed centers of symmetry, requiring the $[Fe_2O_2]$ parallelogram to be planar.[43-46] By contrast, the $\{Fe_2(OMe)_2(O_2CCH_2Cl)\}$ repeating unit in **1** is not centrosymmetric, the dihedral angle across the line joining the two bridging methoxide ligands being 158.8(7)°. The bend at these methoxide bridges correspond to a motion of the iron atoms, hinged at the methoxide bridges, away from the ring center and toward the bridging monochloroacetate ligand, which is the cause of this distortion. If the methoxide hinges were to open fully, a circumstance encountered in most bis(μ-OR)diiron(III) complexes, the Fe···Fe distance in **1** would be approximately 3.08 Å, assuming all other bond lengths to remain constant. This separation is in the range of values reported in Table 3.

Interestingly, the convex bend present across each set of bridging methoxide ligands opposes the overall concave bending curvature of the circle. A quantitative analysis of the angles in **1** reveals that net bending into a circle arises from a larger contribution at the iron centers than at the methoxide hinges. To compare the contribution of the iron sites with those of the methoxide bridges, which are positioned above and below the ring plane, a line joining the oxygen atoms for each set of bridging methoxide ligands was projected onto the plane of ten ferric ions. The calculated positions allow one to evaluate the contribution of the bridging methoxide ligands to the bending of the circle. The 10 iron atoms and intersection points are graphically depicted in Figure 3. The average O′–Fe–O′ angle, where O′ is the intersection point of the projection on the ring, is 119(1)°, and the interior Fe–O′–Fe angle is 205(1)°. For any n-sided regular polygon, the sum of the complements of interior angles must equal 360°. For **1**, which has two types of edges, the circular geometry requires that eq 2 be followed. This relationship holds

$$10[180° - \angle Fe–O'–Fe] + 10[180° - \angle O'–Fe–O'] = 360° \quad (2)$$

exactly for the two observed angles of 119° and 205°. The O′–Fe–O′ angle represents a simple rotation of each iron octahedron about the local C_3 axis, which is approximately parallel to the molecular S_{10} axis. Adjacent metal ions share octahedral faces

(43) (a) Bertrand, J. A.; Breece, J. L.; Kalyanaraman, A. R.; Long, G. J.; Baker, W. A., Jr. *J. Am. Chem. Soc.* **1970**, *92*, 5233. (b) Bertrand, J. A.; Breece, J. L.; Eller, P. G. *Inorg. Chem.* **1974**, *13*, 125. (c) Bertrand, J. A.; Eller, P. G. *Inorg. Chem.* **1974**, *13*, 927. (d) Long, G. J.; Wrobleski, J. T.; Thundathil, R. V.; Sparlin, D. M.; Schlemper, E. O. *J. Am. Chem. Soc.* **1980**, *102*, 6040. (e) Chiari, B.; Piovesana, O.; Tarantelli, T.; Zanazzi, P. F. *Inorg. Chem.* **1982**, *21*, 1396. (f) Barclay, S. J.; Riley, P. E.; Raymond, K. N. *Inorg. Chem.* **1984**, *23*, 2005. (g) Chiari, B.; Piovesana, O.; Tarantelli, T.; Zanazzi, P. F. *Inorg. Chem.* **1984**, *23*, 3398. (h) Walker, J. D.; Poli, R. *Inorg. Chem.* **1990**, *29*, 756. (i) Ménage, S.; Que, L., Jr. *Inorg. Chem.* **1990**, *29*, 4293.

(44) (a) Thich, J. A.; Ou, C. C.; Powers, D.; Vasiliou, B.; Mastropaolo, D.; Potenza, J. A.; Schugar, H. J. *J. Am. Chem. Soc.* **1976**, *98*, 1425. (b) Ou, C. C.; Lalancette, R. A.; Potenza, J. A.; Schugar, H. J. *J. Am. Chem. Soc.* **1978**, *100*, 2053. (c) Borer, L.; Thalken, L.; Ceccarelli, C.; Glick, M.; Zhang, J. H.; Relff, W. M. *Inorg. Chem.* **1983**, *22*, 1719.

(45) (a) Gerloch, M.; Mabbs, F. E. *J. Chem. Soc. A* **1967**, 1900. (b) Ainscough, E. W.; Brodie, A. M.; McLachlan, S. J.; Brown, K. L. *J. Chem. Soc., Dalton Trans.* **1983**, 1385. (c) Olmstead, M. M.; Sigel, G.; Hope, H.; Xu, X.; Power, P. P. *J. Am. Chem. Soc.* **1985**, *107*, 8087. (d) Resce, J. L.; Fanning, J. C.; Day, C. S.; Uhm, S.-J.; Croisy, A. F.; Keefer, L. K. *Acta Crystallogr.* **1987**, *C43*, 2100. (e) Yang, S.-H.; Ladd, J. A.; Goedken, V. L. *J. Coord. Chem.* **1988**, *19*, 235. (f) Kang, B.; Weng, L.; Wu, D.; Huang, L.; Wang, F.; Guo, Z.; Liu, H. *Inorg. Chim. Acta* **1988**, *148*, 147. (g) Snyder, B. S.; Patterson, G. S.; Abrahamson, A. J.; Holm, R. H. *J. Am. Chem. Soc.* **1989**, *111*, 5214. (h) Zlrong, D.; Haltiwanger, R. C.; Bhattacharya, S.; Pierpont, C. G. *Inorg. Chem.* **1991**, *30*, 4288.

(46) (a) Bailey, N. A.; McKenzie, E. D.; Worthington, J. M.; McPartlin, M.; Tasker, P. A. *Inorg. Chim. Acta* **1977**, *25*, L137. (b) Chiari, B.; Piovesana, O.; Tarantelli, T.; Zanazzi, P. F. *Inorg. Chem.* **1982**, *21*, 2444. (c) Chiari, B.; Piovesana, O.; Tarantelli, T.; Zanazzi, P. F. *Inorg. Chem.* **1983**, *22*, 2781. (d) Murch, B. P.; Bradley, F. C.; Boyle, P. D.; Papaefthymiou, V.; Que, L., Jr. *J. Am. Chem. Soc.* **1987**, *109*, 7993. (e) Spartalian, K.; Bonadies, J. A.; Carrano, C. J. *Inorg. Chim. Acta* **1988**, *152*, 135. (f) Brennan, B. A.; Chen, Q.; Juarez-Garcia, C.; True, A. E.; O'Connor, C. J.; Que, L., Jr. *Inorg. Chem.* **1991**, *30*, 1937.

(47) (a) Anderson, B. F.; Buckingham, D. A.; Robertson, G. B.; Webb, J.; Murray, K. S.; Clark, P. E. *Nature* **1976**, *262*, 722. (b) Anderson, B. F.; Webb, J.; Buckingham, D. A.; Robertson, G. B. *J. Inorg. Biochem.* **1982**, *16*, 21.

Table 3. Comparison of Bond Distances (Å) and Angles (deg) for Complexes Having $\{Fe_2(OR)_2(O_2CR)\}^{3+}$ and $\{Fe_2(OR)_2\}^{4+}$ Cores[a]

molecular formula	core structure	Fe–OR	Fe–(OR)–Fe	(RO)–Fe–(OR)	Fe···Fe	ref
1	$\{Fe_2(OMe)_2(O_2CCH_2Cl)\}^{3+}$	1.975(4)	99.7(5)	78.0(2)	3.028(4)	*b*
$[Fe_2(cat)_4(OAc)]^{3-}$ [c]	$\{Fe_2(OAr)_2(OAc)\}^{3+}$	2.02(4)	103(1)	71.9(4)	3.15(5)	47
$[Fe(OEt)Cl_3]_2$ [d]	$\{Fe_2(OEt)_2\}^{4+}$	1.98(5)	107.0(3)	73.0(3)	3.117	43h
$[Fe(OEt)(acac)_2]_2$	$\{Fe_2(OEt)_2\}^{4+}$	1.982(4)	103.6(3)	76.4(2)	3.116(1)	43g
$[Fe(salpa)Cl]_2$	$\{Fe_2(OR)_2\}^{4+}$	1.96(4)	104.1(6)	75.9(6)	3.089(6)	43a,b
$[Fe_2(salpa)_2(salpaH)_2]$	$\{Fe_2(OR)_2\}^{4+}$	1.97(3)	109(2)	70.6(5)	3.217(7)	43c
$[Fe(N(PL)_2ala)]_2^{2+}$	$\{Fe_2(OR)_2\}^{4+}$	2.02(2)	103.8(2)	76.2(2)	3.180(3)	43d
$[Fe(OH)(H_2O)(dipic)]_2$	$\{Fe_2(OH)_2\}^{4+}$	1.97(4)	103.6(2)	76.4(2)	3.089(2)	44a
$[Fe(OH)L]_2$	$\{Fe_2(OH)_2\}^{4+}$	2.02(5)	102.8(3)	77.2(3)	3.155(3)	44c
$[Fe(biphen)_2]_2^{2-}$ [d]	$\{Fe_2(OAr)_2\}^{4+}$	2.01(6)	108.0(4)	72.0(1)	3.255	45b

[a] All distances were averaged for each metrical parameter where appropriate, with the number in parentheses being the estimated standard deviation. [b] This work. [c] See footnote 27 for abbreviations. [d] The iron atoms in these complexes are five-coordinate.

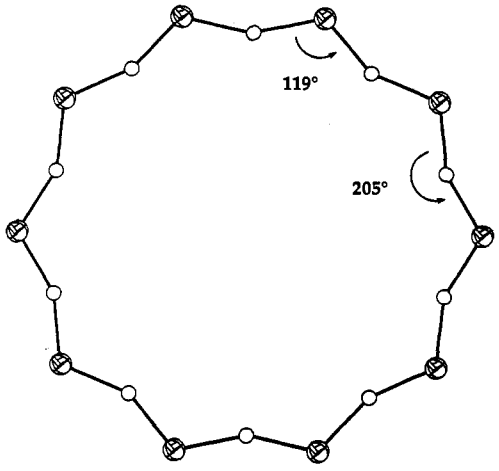

Figure 3. Ring geometry of **1** viewed perpendicular to the plane of iron atoms. Cross-hatched spheres are the iron atoms and open circles are bridging methoxides (O′) projected onto the plane of the iron atoms, as described in the text. The interior angles of 119° and 205° refer to O′–Fe–O′ and Fe–O′–Fe, respectively.

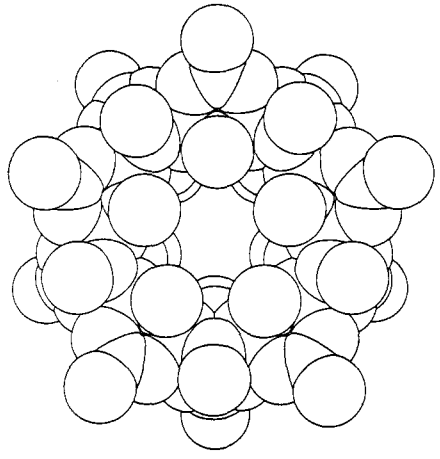

Figure 4. Space-filling representation of the structure of **1** viewed perpendicular to the plane of iron atoms. Hydrogen and chlorine atoms are omitted for clarity. The diameter of the hole is 2–3 Å.

so the contributions from each iron site are additive. It is therefore clear that the combination of a complex and yet subtle balance between the iron and alkoxide bridge geometries affords the beautiful circular geometry of the ferric wheel.

As is evident from the space-filling view shown in Figure 4, complex **1** has a small central hole, with an approximate diameter of 2–3 Å. In the final difference Fourier map, some residual electron density, 0.8 $e^-/Å^3$, was located at the special position in the center of the ring. The small interior of **1**, together with the negligible electron density located there, indicates that no guest molecule is present. A unit cell packing diagram (Figure S3, supplementary material) reveals that the molecules stack along the *c* axis with their interior holes overlapping to some degree, so that an infinite channel is generated in the crystal lattice. A stereoview down *c* highlighting this feature is available (Figure S4, supplementary material).

The planar ring structure of **1** is unique in iron–oxygen chemistry. Almost all polyiron complexes with six or more metal atoms have a three-dimensional core comprised of at least one bridging O^{2-} ion.[7-12] A few two-dimensional arrays are known, however. Six of the eight ferric ions in $[Fe_8(O)_2(OH)_{12}(Me_3tacn)_6]^{8+}$ are approximately coplanar.[8] A single iron–oxo–hydroxo layer also forms in two polyiron complexes which cocrystallized from aqueous solutions of ferric nitrate and the ligand H_3heidi.[12] The central cores of $[Fe_{19}(O)_6(OH)_{14}(heidi)_{10}(H_2O)_{10}]^+$ and $[Fe_{17}(O)_4(OH)_{16}(heidi)_8(H_2O)_{12}]^{3+}$ can be considered segments of an infinite two-dimensional array of the hypothetical ferric hydroxide species, $\{Fe(OH)_2\}^+$. A decanuclear manganese compound, $[Mn_{10}O_{14}(tren)_6]^{8+}$, also belongs to the AX_2 structural class,[48] of which the extended structures of CdI_2 and $Mg(OH)_2$ are solid-state examples. The circular structure of **1**, although planar, differs dramatically from those of these two-dimensional complexes.

Considering other metal ions and bridging atoms, however, a cyclic arrangement of metal ions and ligand atoms is not so uncommon. Some prominent representatives, each of which has at least eight metal ions and a circular framework, include $[CrF(O_2CCMe_3)_2]_8$,[49] the α- and β-forms of $[Na_2Fe_{18}S_{30}]^{8-}$ and $[Na_9Fe_{20}Se_{38}]^{9-}$,[28] $[Ni(SCH_2CO_2Et)_2]_8$,[50] $[Cu(OH)(dmpz)]_8$,[51] and $[Y(OCH_2CH_2OMe)_3]_{10}$.[52] Several of these complexes contain guest molecules in their interiors which form secondary bonding interactions with the bridging atoms of the rings. Such stabilizing interactions are distinct from the template effect of an organic guest molecule that coordinates to the metal ions in the ring, as occurs for numerous polyoxo early transition metal complexes.[53] Although these cyclic molecules have a variety of different metal coordination numbers and bridging ligands, a few broad generalizations concerning their structures can be made. All of the complexes, except for the iron–sulfur and –selenium complexes, have idealized $D_{(n/2)d}$ point symmetry, where *n* is the total number of metal ions in the circle. The molecules have toroidal structures with interior cavity dimensions that depend on the identity of the bridging ligands. The number of repeat units in each molecule varies with the metal and bridge geometries. As revealed by the foregoing curvature analysis for the ferric wheel, subtle factors combine to produce the observed ring architectures.

(48) Hagen, K. S.; Armstrong, W. H.; Olmstead, M. M. *J. Am. Chem. Soc.* **1989**, *111*, 774.
(49) Gérbéléu, N. V.; Struchkov, Y. T.; Timko, G. A.; Batsanov, A. S.; Indrichan, K. M.; Popovich, G. A. *Dokl. Akad. Nauk SSSR* **1990**, *313*, 232.
(50) Dance, I. G.; Scudder, M. L.; Secomb, R. *Inorg. Chem.* **1985**, *24*, 1201.
(51) Ardizzoia, G. A.; Angaroni, M. A.; La Monica, G.; Cariati, F.; Cenini, S.; Moret, M.; Masciocchi, N. *Inorg. Chem.* **1991**, *30*, 4347.
(52) Poncelet, O.; Hubert-Pfalzgraf, L. G.; Daran, J.-C.; Astier, R. *J. Chem. Soc., Chem. Commun.* **1989**, 1846.
(53) For example, see: Chen, Q.; Liu, S.; Zubieta, J. *Angew. Chem., Int. Ed. Engl.* **1988**, *27*, 1724.

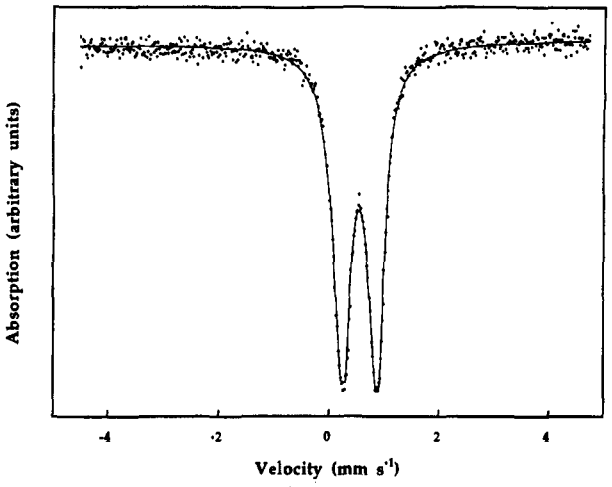

Figure 5. Mössbauer spectrum of polycrystalline **1** at 4.2 K. The solid line is the best fit to the data with the spectral parameters listed in Table 4.

Mössbauer Spectroscopy. The solid-state Mössbauer spectrum of **1** measured at 4.2 K is shown in Figure 5. A single quadrupole doublet occurs for the five unique iron sites, as expected from the D_{5d} molecular symmetry. No magnetic hyperfine interactions were observed in zero applied field. The spectral parameters calculated for a single site fit to the spectrum of **1** are reported in Table 4, along with the analogous data for several diiron(III) complexes.[43-46] An isomer shift of 0.52 mm s^{-1} is characteristic of high-spin ferric ions. The quadrupole splitting parameter of 0.62 mm s^{-1} indicates a slightly unsymmetrical electric field, consistent with the 0.1-Å variations in Fe–O bond distances revealed by the X-ray investigation. A width at half-height of 0.36 mm s^{-1} for the quadrupole doublet is reasonable. The Mössbauer values of **1** are consistent with those of other bis(μ-OR)diiron(III) complexes, and the ring geometry does not appear to affect the nuclear transition.

Magnetic Studies. The temperature dependence of the molar magnetic susceptibility of **1** is depicted in Figure 6. The susceptibility, measured at 3 kG, increases below 300 K, reaches a maximum at 65 K, and decreases rapidly at lower temperatures. This behavior is characteristic of antiferromagnetic exchange coupling, a feature common to most polynuclear iron complexes. The magnitude of χT for the complex decreases from 32.3 emu mol^{-1} K at 300 K to 0.355 emu mol^{-1} K at 2.5 K. The calculated spin-only value for ten independent $S_i = {}^5/_2$ ions with $g = 2.0$ is 43.8 emu mol^{-1} K, where S_i is the spin of the ith ion in the cluster. The spin states for the molecule can have integer values from 0 to 25, resulting in a total number of magnetic states of 6^{10}, or 6.04×10^7.

Except for the very low temperature data, the temperature dependence of the magnetic susceptibility is typical of a Heisenberg chain of antiferromagnetically coupled $S_i = {}^5/_2$ ions.[54,55] Quantitative least-squares fitting of the susceptibility data above 14 K for **1** using the classical spin treatment gave an exchange interaction parameter J of approximately 10 cm^{-1} with the Hamiltonian $JS_i \cdot S_{i+1}$ and $g = 2.0$. The calculated χ values are shown as a dashed line in Figure 6. Because the spins are not quantized in this model, the susceptibility does not approach zero at low temperatures, and in general, this treatment is more accurate when J/kT is not too large. Nevertheless, this classical theory provides an initial estimate of the nearest-neighbor exchange interaction constant in **1**.

Although many calculations have been performed on rings of spins,[54] a quantum mechanical evaluation of a system containing ten $S_i = {}^5/_2$ ions is to our knowledge impossible with present computers. The energies of spin states ranging from $S = 0$ to 25 must be calculated, with matrices to be diagonalized as large as 484 155 for $S = 5$. Some of us have recently advocated the use of irreducible tensor operators for calculating the energy levels,[56] but even with the aid of point group symmetry one can only perform the computations on rings containing up to eight $S_i = {}^5/_2$ spins.[57] It is possible, however, to use the method to obtain a reasonably good value for the coupling constant J in **1** with the assumption of Heisenberg-like exchange.

Figure 7 plots the reduced susceptibility, $\chi|J|/g^2N\mu_B$, as a function of the reduced temperature, $kT/|J|$, for rings of four, six, and eight $S_i = {}^5/_2$ ions. Spin frustration occurs in rings with an odd number of ions, and they are not treated here. The spin Hamiltonian shown in eq 3 was employed, where n is the number

$$H = \sum_{i=1}^{n-1} JS_i \cdot S_{i+1} + JS_1 \cdot S_n \qquad (3)$$

of ions in the ring, the $S_i \cdot S_{i+1}$ term describes the nearest-neighbor interactions, and the $S_1 \cdot S_n$ component accounts for ring closure. It is apparent from the plot that, with increasing numbers of ions, the reduced susceptibility converges, indicating that the magnetic properties of **1** should be reasonably well approximated by the results for an octamer. The energy levels of the 8-spin ring were therefore used to fit the experimental susceptibility of the 10-iron ferric wheel. Calculations were carried out with J values ranging from 8 to 11 cm^{-1} in steps of 0.2 cm^{-1}, and the residuals were computed. The best fit, shown as a solid line in Figure 6, has $J = 9.6$ cm^{-1} with $g = 2.0$. This analysis reproduces the higher temperature susceptibility data quite well but does not account for the plateau at 5 K. Calculations using models with alternating exchange constants or with next nearest-neighbor interactions included in the Hamiltonian were investigated in an effort to understand the low-temperature discontinuity. Neither model was able to reproduce this feature, however. It may be due to an impurity, possibly a diiron(III) complex, or to intercluster coupling along the direction of the stacks of **1** in the crystal lattice. An impurity would be consistent with small differences observed in the susceptibility for this temperature regime for several different samples.

The energy values for the lowest-lying spin states in **1** can be calculated by using the exchange constant J for the eight-membered ring, and they are plotted in Figure 8 for $S = 0$ to 4 and with $E < 100$ cm^{-1}. It is immediately apparent that the levels are quite close in energy, as expected from the relatively small exchange constant and the large density of states. At first glance, the room temperature value of χT appears to be too low for the relatively small magnitude of J. In such a large cluster, however, the energy levels arising from even a small exchange constant will be distributed over a significant range. Some proportion of states therefore have zero or only a small thermal population, even at temperatures as high as 300 K, which suppresses the observed magnetism. The exchange constant for **1** falls at the lower end of the range, 10–50 cm^{-1}, previously established for bis(μ-OR)diiron(III) complexes, as shown in Table 4. The Fe–OR–Fe angle in **1** is substantially smaller than those realized in the rest of the series, suggesting that it therefore may be a relevant parameter in the exchange mechanism.

Magnetization measurements of **1** made at 4.2 and 0.6 K in applied magnetic fields of up to 20 T are shown in Figures 9 and 10, respectively. The 4.2 K data increase smoothly in magnetization with no indication of saturation. By contrast, the data at 0.6 K increase in a stepwise fashion. Between 0 and 4 T, the magnetization is quite small, after which it increases to approximately 2 μ_B, corresponding to an $S = 1$ state. At approximately 9.2 T, a second inflection point occurs, increasing the magne-

(54) Bonner, J. C.; Fisher, M. E. *Phys. Rev.* **1964**, *135*, A640.
(55) Witteveen, H. T.; Reedijk, J. *J. Solid State Chem.* **1974**, *10*, 151.
(56) Gatteschi, D.; Pardi, L. *Gazz. Chim. Ital.* **1993**, *123*, 231.
(57) Delfs, C. D.; Gatteschi, D.; Pardi, L.; Sessoli, R.; Wieghardt, K.; Hanke, D. *Inorg. Chem.* **1993**, *32*, 3099.

Table 4. Comparison of Mössbauer Spectral Parameters (mm s^{-1}) and Magnetic Exchange Constants (J, cm^{-1}) for Complexes Having $\{Fe_2(OR)_2(O_2CR)\}^{3+}$ and $\{Fe(OR)_2\}^{4+}$ Cores

		Mössbauer parameters[a]					
molecular formula	core structure	T (K)	δ[b]	ΔE_Q	Γ	exchange constant, J[c]	ref
1	$\{Fe_2(OMe)_2(O_2CCH_2Cl)\}^{3+}$	4.2	0.52	0.62	0.36	9.4	*d*
$[Fe(OEt)Cl_3]_2$[e]	$\{Fe_2(OEt)_2\}^{4+}$	*f*				49.2	43h
$[Fe(OEt)(acac)_2]_2$[g]	$\{Fe_2(OEt)_2\}^{4+}$	*f*				22.0	43g
$[Fe(salpa)Cl]_2$	$\{Fe_2(OR)_2\}^{4+}$	78	0.44	1.03	0.26	34	43a,b
$[Fe(N(PL)_2ala)]_2^{2+}$	$\{Fe_2(OR)_2\}^{4+}$	78	0.51	0.83	0.58	10.4	43d
$[Fe(OH)(H_2O)(dipic)]_2$	$\{Fe_2(OH)_2\}^{4+}$	*f*				22.8	44a
$[Fe(OH)L]_2$	$\{Fe_2(OH)_2\}^{4+}$	4.3	0.49	0.56	0.34	20.8	44c
$[Fe(biphen)_2]_2^{2-}$[e]	$\{Fe_2(OAr)_2\}^{4+}$	300	0.46	0.65	*f*	28	45b

[a] Mössbauer spectral parameters: δ, isomer shift; ΔE_Q, quadrupole splitting; Γ, width at half peak height. [b] Referenced versus iron foil at 300 K. [c] The Hamiltonian JS_iS_{i+1} was employed to report the magnetic exchange interactions. [d] This work. [e] The iron atoms in these complexes are five-coordinate. [f] Not reported. [g] See ref 27 for abbreviations.

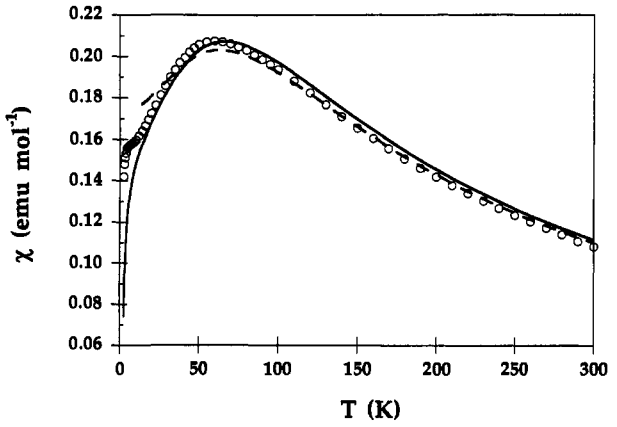

Figure 6. Plot of molar susceptibility, χ (emu mol^{-1}), versus temperature (K) for **1**. The experimental data, measured at 3 kG, are shown as open circles. The dashed and solid lines are the antiferromagnetic Heisenberg chain and quantum mechanical fits, respectively (see text).

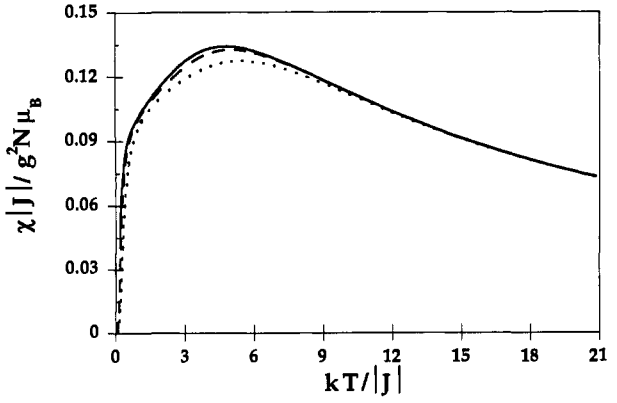

Figure 7. Plot of calculated reduced susceptibility per ion versus the reduced temperature for rings composed of four (···), six (– –), and eight (—) $S_i = {}^5/_2$ ions.

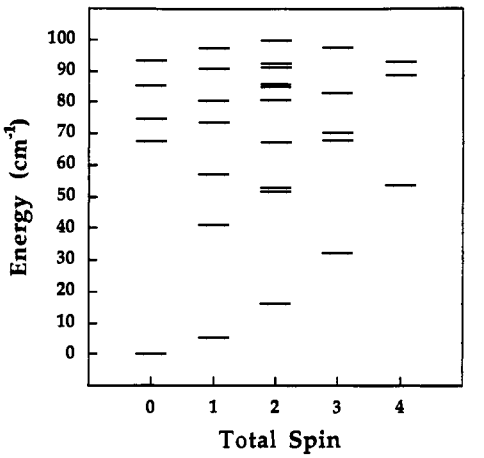

Figure 8. Calculated energies for the lowest-lying spin states of **1** grouped for clarity by their respective S values.

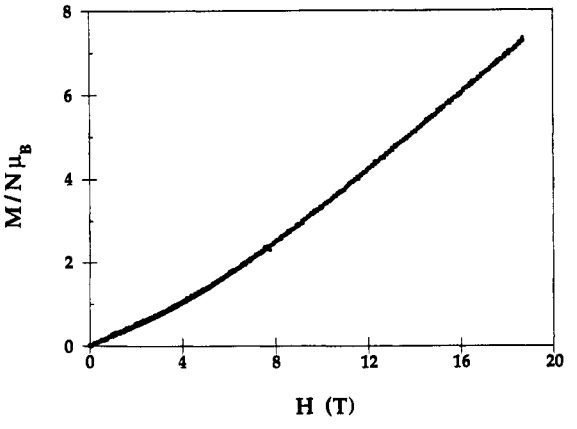

Figure 9. Plot of reduced magnetization, $M/N\mu_B$, versus field, H (tesla), for **1** at 4.2 K. The experimental data, shown as filled circles, and the least-squares fit, drawn as a solid line, are indistinguishable.

tization to 4 μ_B ($S = 2$). This pattern is repeated, the final magnetic field of 19 T producing a net magnetization of 7.2 μ_B. The width of these transitions is independent of the applied magnetic field, whereas the slopes at the plateaus appear to increase slightly with higher fields.

This magnetization behavior strongly supports the model used to evaluate the variable-temperature susceptibility. The steps observed in the 0.6 K data originate from crossovers of higher spin multiplets at larger applied fields. At zero-field, the $|S = 0, M = 0\rangle$ state is lowest in energy. With increasing field, however, a magnetic subcomponent of the first excited state having a non-zero spin, in this case $S = 1$ as indicated in Figure 8, drops in energy according to $-g\mu_B H$, becoming the ground state at approximately 4.6 T. The $|0, 0\rangle$ and $|1, -1\rangle$ states have the same energy when the relationship in eq 4 is satisfied. At higher fields,

$$H_{0,1} = [E(1) - E(0)]/g\mu_B \quad (4)$$

the magnetization saturates at the value expected for the $|1, -1\rangle$ component, or 2 μ_B. In a similar manner, the $|2, -2\rangle$ level eventually crosses the $|1, -1\rangle$ state, since it decreases in energy at a steeper rate with respect to H, $-2g\mu_B H$ versus $-g\mu_B H$. This pattern is repeated with the $|S, -S\rangle$ subcomponents of the $S = 3$ and 4 excited spin levels, as presented graphically in Figure 11. These crossover transitions are observed at 0.6 K because only the lowest spin level is thermally populated at this temperature. At 4.2 K, these steps are thermally broadened and several of the excited spin states contribute to the observed magnetization, thereby obscuring the stepwise nature of the ground-state change. Fortuitously, the magnitude of the exchange constant J, the low temperature employed, and the availability of the large magnetic fields allow these steps to be resolved for **1**.

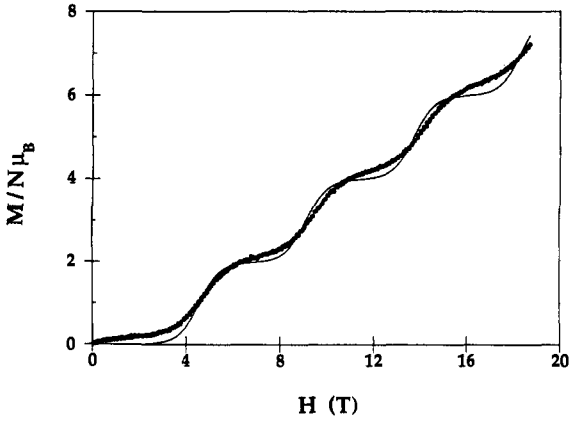

Figure 10. Plot of reduced magnetization, $M/N\mu_B$, versus field, H (tesla), for **1** at 0.6 K. The experimental data are shown as filled circles and the least-squares fit is drawn as a solid line.

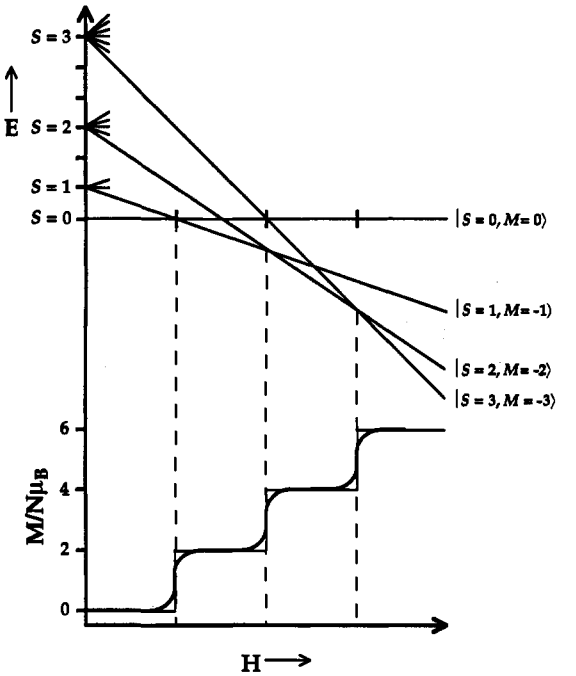

Figure 11. Spin crossover diagram for the first four spin levels of **1**.

The general expression for the crossover transition between the S and $S+1$ levels is given in eq 5. To a good approximation,

$$H_{S,S+1} = [E(S+1) - E(S)]/g\mu_B \quad (5)$$

the difference between $H_{S,S+1}$ and $H_{(S-1),S}$ is constant. The separation between the S and $S+1$ state is therefore $(S+1)P$, where P is a common energy parameter, which means that the energy of the lowest state for each S value follows the simple Landé interval rule, eq 6. This behavior can be understood by

$$\mathrm{E}(S) = (\mathrm{P}/2)S(S+1) \quad (6)$$

considering that the lowest, $S = 0$ state of a ring of $2N$ spins may be expressed by a spin configuration in which the odd site spins are up and the even site spins are down. The former give $S_A = NS_i$, and the latter produces $S_B = NS_i$. Combining these intermediate spins S_A and S_B, the energies of the total spin states $S_A - S_B \leq S \leq S_A + S_B$ are given by eq 7. The repetitive nature of the cross-over points observed with increasing field for **1** is in agreement with this expression.

$$E(S) = (P/2)[S(S+1) - 2NS_i(NS_i+1)] \quad (7)$$

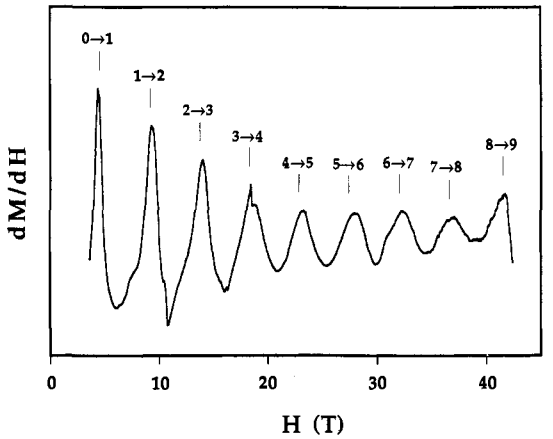

Figure 12. Differential magnetization dM/dH for **1** measured in a decreasing field. The crossovers between the S, $(S+1)$ spin states are noted above each maximum. The vertical lines correspond to the calculated field for each transition using a P value of 4.27 cm^{-1} as described in the text.

For a ring of $2N$ spins, the effective parameter P, to the level of the approximation used, can be related to the exchange constant J by a simple expression derived from irreducible tensor operators, eq 8. The validity of this relationship has been evaluated for

$$P = \frac{2}{N}J \quad (8)$$

complexes with $N = 2$, 3, and 4 for which we have performed both the complete calculations and those corresponding to the approximation of eq 8. Inspection of the matrix elements involving these spin functions reveals that the ratio between the diagonal and off-diagonal elements is small, hence only a small amount of mixing of other spin functions into the lowest state occurs for a given S value. This result is also confirmed by inspection of the eigenvectors. Ignoring small matrix elements in order to obtain approximate eigenvalues from large matrices is a procedure employed previously, but not in such a crude manner.[58] The approximation becomes less accurate when S_i is small, because the ratio between the diagonal and off-diagonal matrix elements is less favorable.

Fits to the 0.6 and 4.2 K magnetization data of **1** gave a parameter P of 4.27 and 4.24 cm^{-1}, respectively. As revealed in the two figures, the agreement between the calculated and experimental data is excellent. The deviations observed in the 0.6 K magnetization may be due to the presence of zero field splitting of the S states, for such anisotropy would broaden the transitions, or the presence of some impurity. The P values correspond to $J \sim 10$ cm^{-1} according to eq 8 where $N = 5$, which is consistent with the coupling constant determined from the variable-temperature magnetic data. An identical value for the exchange constant in **1** has therefore been determined from two different experiments and theoretical analyses.

By using even larger magnetic fields, crossover transitions for states with S greater than 4 were observed for **1**. A pulsed differential magnetization study, which gives the change in magnetization with respect to field, dM/dH, as the field varies, was conducted. With a unique instrumental setup, a pulsed field from 0 to 50 T was applied with a starting temperature of 0.6 K.[23] The data are presented in Figure 12, along with the predicted magnetic field value for each crossover transition. The latter were calculated by substituting eq 6 into eq 5 and by using a P value of 4.27 cm^{-1}. Nine discrete maxima, which correspond to ground-state transitions from $|S, -S\rangle$ to $|S+1, -(S+1)\rangle$ with S ranging from 0 to 8, are realized. The dM/dH data shown in Figure 12 have an amplitude that decreases with increasing field

(58) Hauser, U.; Gudel, H. U. *Theor. Chim. Acta* **1983**, *62*, 319.

and a variation in the width of the transition, whereas the width and amplitude of the DC magnetization data in Figure 10 are constant up to 20 T. Examination of dM/dH for the pulsed experiment indicates pronounced narrowing of the transition at low field. Narrowing has been previously observed and discussed for dilute magnetic semiconductors in pulsed fields.[59]

The $|S, -S\rangle$ to $|S + 1, -(S + 1)\rangle$ transitions occur at regular intervals and are found at the expected magnetic fields for the value of P determined from the DC magnetization experiments. The spacing in the spin manifold of **1** is therefore highly conserved, even for higher excited states. Previously, the greatest number of transitions observed in related experiments was five, for a manganese(II) dimer doped in a semiconductor matrix.[23] The result corresponded to all of the 5 potential spin crossovers for the system, which has a maximum $S = 5$. In the case of **1**, however, with a 50 T magnetic field and an exchange constant of 9.4 cm^{-1}, 9 of the possible 25 steps were observed. These results confirm quite dramatically the theoretical description of the magnetic properties of the ferric wheel.

Concluding Remarks

The methanolysis of basic iron monochloroacetate and ferric nitrate produces a molecular ferric wheel, $[Fe(OMe)_2(O_2CCH_2Cl)]_{10}$ (**1**). This decanuclear iron(III) complex has a unique and aesthetically pleasing[60] circular structure previously unknown in iron–oxygen chemistry. The ring structure results from constructive (concave) and destructive (convex) curvatures that have been traced to specific geometric features of the tribridged metal ion pairs. From comparisons with other (μ-OR)diiron(III) complexes, we conclude that the coordination geometry and Mössbauer properties for the individual iron sites in the wheel are not greatly affected by the circular structure. From variable-temperature magnetic studies, a single antiferromagnetic exchange coupling constant J of 9.4 cm^{-1} was determined for nearest-neighbor interactions. DC magnetization and pulsed magnetic field experiments have verified this value. In many ways, the magnetic properties of **1** are similar to those observed for a simple dimetallic center, and no unusual effects, such as spin frustration, are present. For this molecule, however, S can adopt integer values from 0 to 25, revealed dramatically by the field-dependent magnetic studies at 0.6 K. These results confirm the theoretical analyses derived for rings of metal ions, which have been extrapolated to evaluate the magnetic properties of one-dimensional systems.

(59) (a) Shapira, Y.; Foner, S.; Heiman, D.; Wolff, P. A.; McIntyre, C. R. *Solid State Commun.* **1989**, *71*, 355. (b) Bindilatti, V.; Vu, T. Q.; Shapira, Y. *Solid State Commun.* **1991**, *6*, 423.

(60) Hoffmann, R. *Sci. Am.* **1993**, *268*, 66.

Acknowledgment. This work was supported by grants from the National Institute of General Medical Sciences, the National Science Foundation, and the Office of Naval Research. The Francis Bitter National Magnet Laboratory was supported by the National Science Foundation. K.L.T. is grateful to the National Science Foundation for a Graduate Research Fellowship. E. J. McNiff, Jr., of the Francis Bitter National Magnetic Laboratory is thanked for carrying out the DC magnetization studies, and Dr. A. Masschelein is acknowledged for obtaining the resonance Raman spectrum. Professor A. Bino of the Hebrew University is thanked for his synthetic insight, and Professor R. J. Silbey of M.I.T. and Professor S. Geschwind of Clark University are also acknowledged for helpful discussions concerning the magnetic features of the ferric wheel.

Supplementary Material Available: Tables of atomic positional parameters, anisotropic temperature factors, bond distances and angles, and variable-temperature magnetic data for **1**, electronic and resonance Raman spectra of the methanol solution used in the preparation of **1**, and two stereoviews of the crystal lattice of **1** (14 pages). This material is contained in many libraries on microfiche, immediately follows this article in the microfilm version of the journal, and can be ordered from the ACS; see any current masthead page for ordering information.